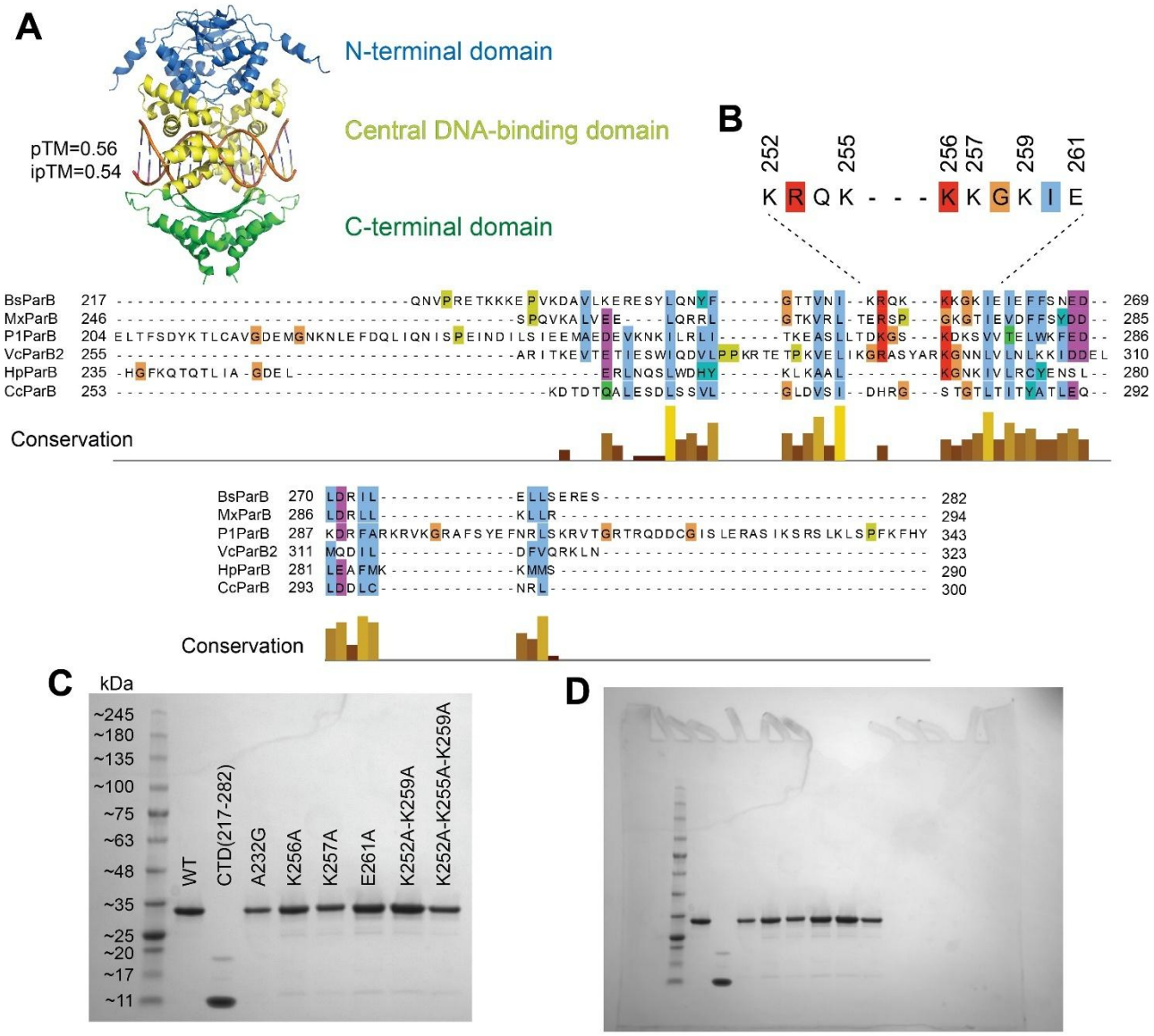

Figure S1. *Bacillus subtilis* ParB used in this study and a ParB sequence alignment.

(**A**) AlphaFold 3 [1] prediction of *B. subtilis* ParB structure. Three distinct domains are shown in colors. Blue: N-terminal domain (NTD), Yellow: Central DNA-binding domain (CDBD), Green: C-terminal domain (CTD). A 16-basepair double-stranded *parS* DNA (TGTTCCACGTGAAACA) on CDBD is also shown. pTM and ipTM refer to the predicted template modeling and the interface predicted template modeling scores, respectively.

(**B**) Multiple Alignment using Fast Fourier Transform (MAFFT) for several ParB CTD homologues via the EMBL-EBI Job Dispatcher sequence analysis tool [2] and visualized with Jalview (red: positively charged, magenta: negatively charged, blue: hydrophobic, green: polar, cyan: aromatic, glycine: orange, Proline: light green) [3]. Bs (Accession number: P26497): *Bacillus subtilis*, Mx (Q1CVJ4): *Myxococcus xanthus*, P1 (P07621): P1 plasmid, Vc (Q9KKJ3): *Vibrio cholerae*, Hp (O25758): *Helicobacter pylori*, Cc (B8GW30): *Caulobacter crescentus*. The amino acid sequences of BsParB used in this study are enlarged at the top.

(**C**) SDS-PAGE gel image for a protein ladder (left) and purified *B.* ParB (BsParB) proteins used in this study.

(**D**) Raw SDS-PAGE gel image.

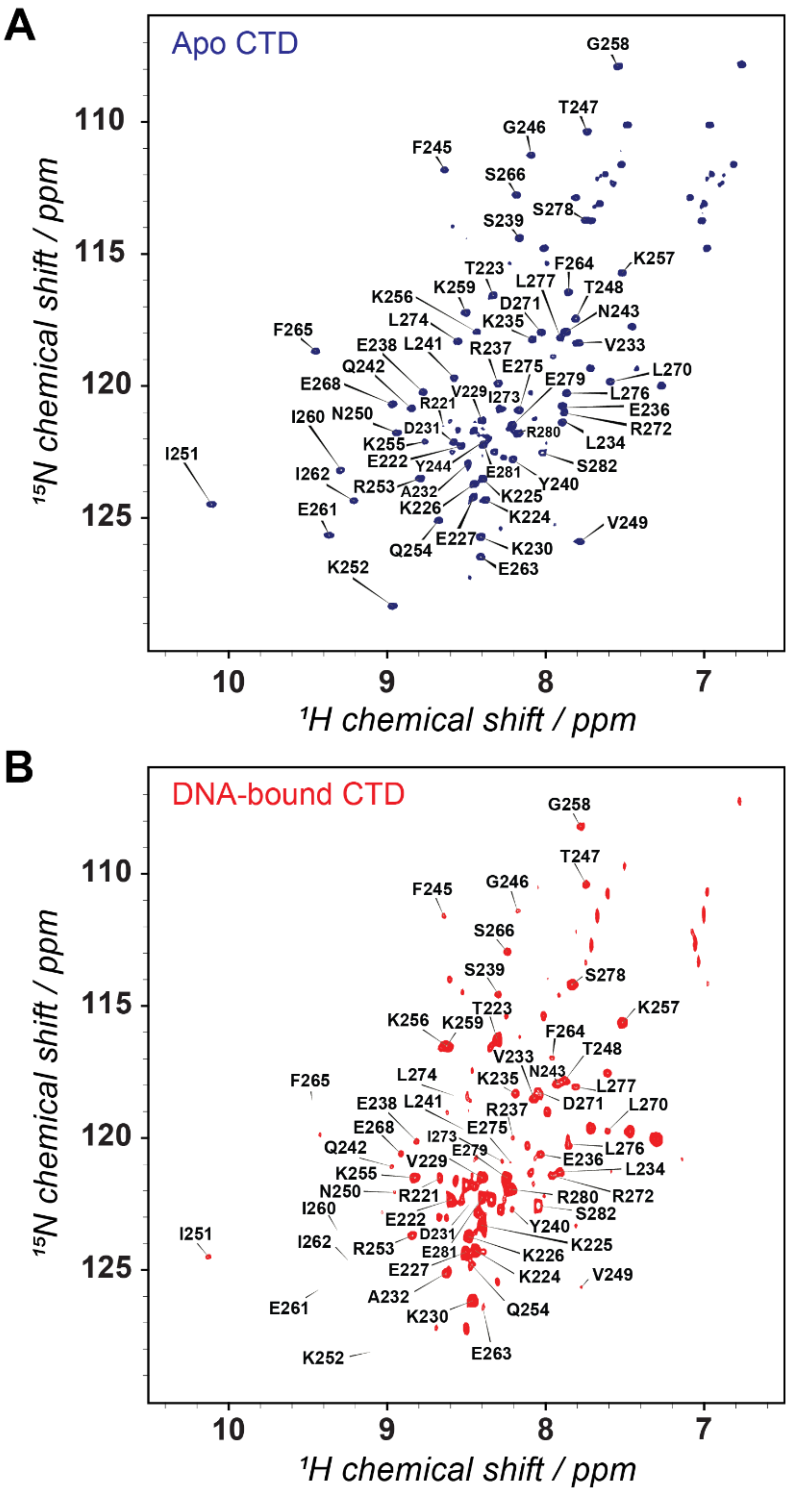

Figure S2. ^{1}H-^{15}N heteronuclear single quantum coherence (HSQC) spectra of the *Bacillus subtilis* ParB C-terminal domain (CTD)

(**A**-**B**) ^{1}H-^{15}N HSQC spectra of apo-CTD and 1.25 equivalent DNA-bound CTD ([DNA] / [CTD] = 1.25), respectively, at 11.7 T. 400 μM CTD in PBS buffer, pH 6.1 at 308 K. While most signals were resolved, the significant exchange broadening led to non-observable signals from G216, Q217, and N218.

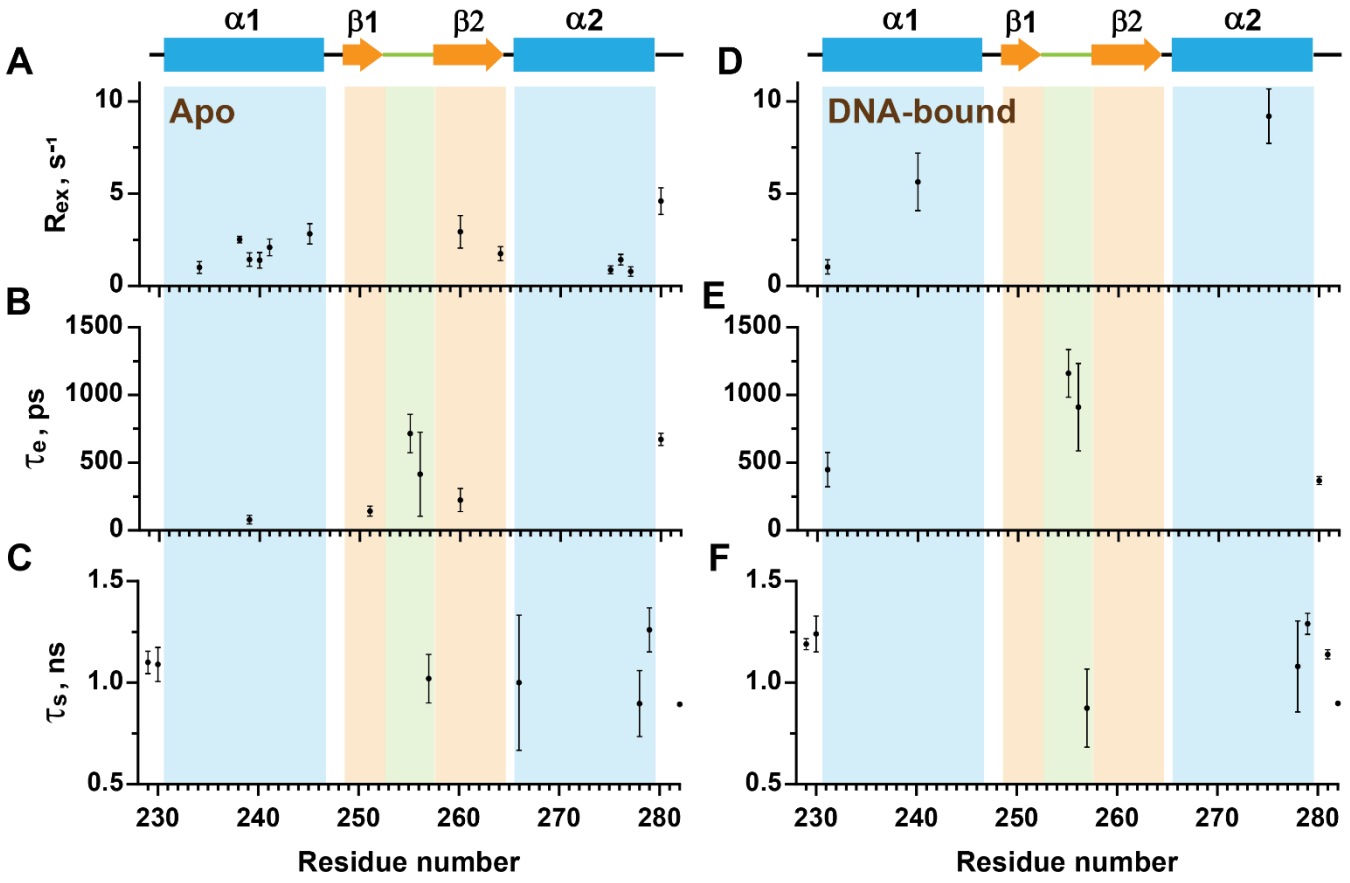

Figure S3. Parameters defining the backbone dynamics of apo and DNA-bound CTD, obtained from model-free analyses, as a function of residue number

(**A**-**C**) Backbone dynamics parameters for apo CTD. R_{ex}, τ_e, and τ_s are the chemical exchange contribution, the internal correlation time, and the residue with internal correlation times at slower timescales, respectively. The secondary structure determined from the NMR structure (PDB: 5NOC) is displayed at the top: α-helices (cyan bars), β-strands (light orange arrows), loop regions (black lines), and linker region (light green).

(**D**-**F**) Backbone dynamics parameters for DNA-bound CTD.

Error bars: standard deviation (SD)

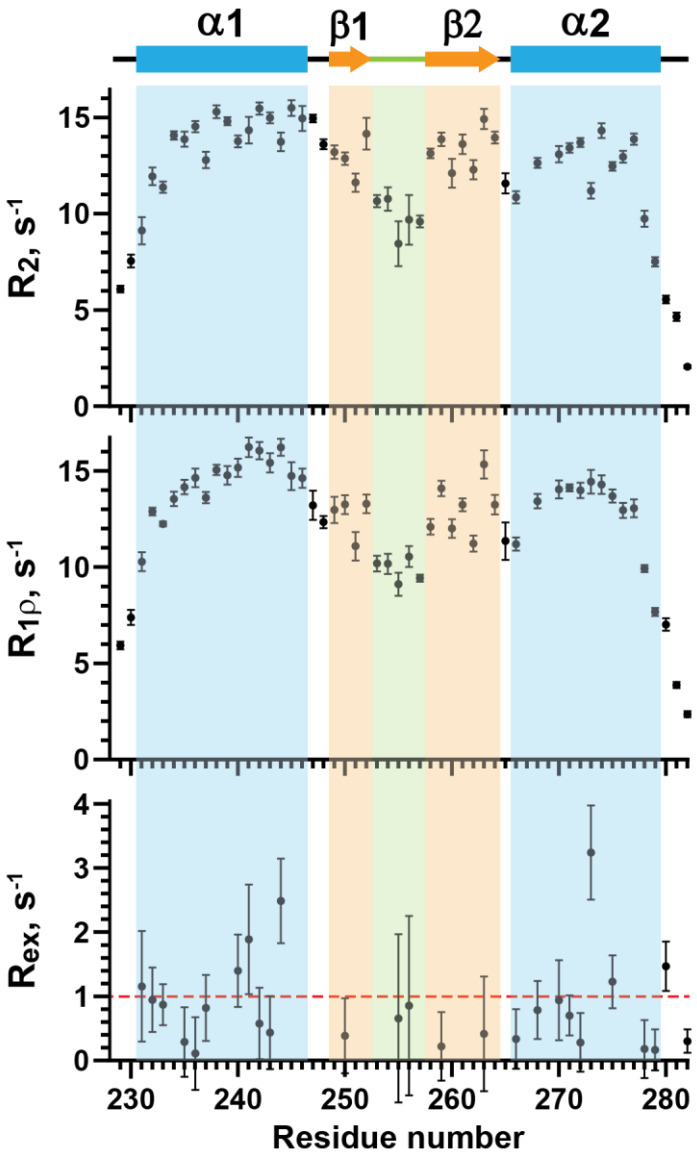

Figure S4. Experimentally determined R_2, $R_1\rho$, and R_{ex} values of apo CTD at 16.4 T.

From the top, R_2, $R_1\rho$, and R_{ex} values as a function of residue numbers. R_{ex} values were obtained by subtracting $R_1\rho$ from R_2. Negative R_{ex} values corresponding to noise were omitted in the graph for clarity. Red dotted line (R_{ex}=1) is shown for visual guidance. 290 μM CTD in PBS buffer, pH 6.1 at 308 K.

Error bars: standard deviation (SD)

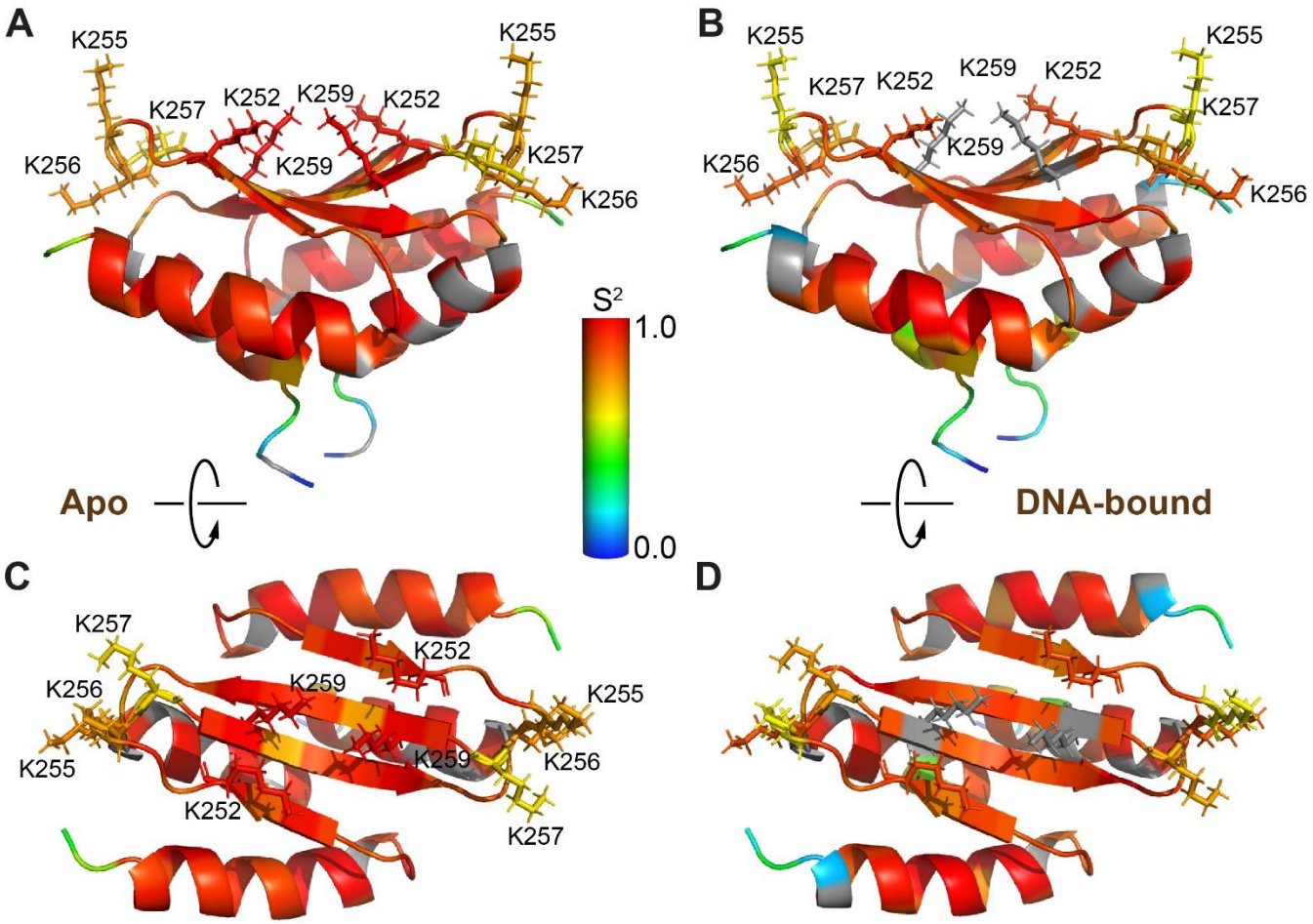

Figure S5. Experimentally determined S^2 mapped onto an NMR structure of CTD (PDB entry: 5NOC) (**A** and **B**) Color-coded S^2 values from NMR relaxation experiments for (**A**) apo and (**B**) DNA-bound CTD, respectively. Lysines of interest are labeled. These two panels are identical to Figures 2C and 2D panels. (**C** and **D**) Views from the top by rotating (**A**) and (**B**) by 90°, respectively. Color scheme: gradient from blue to red for residues with S^2 between 0.0 and 1.0, and gray for residues with no assigned S^2.

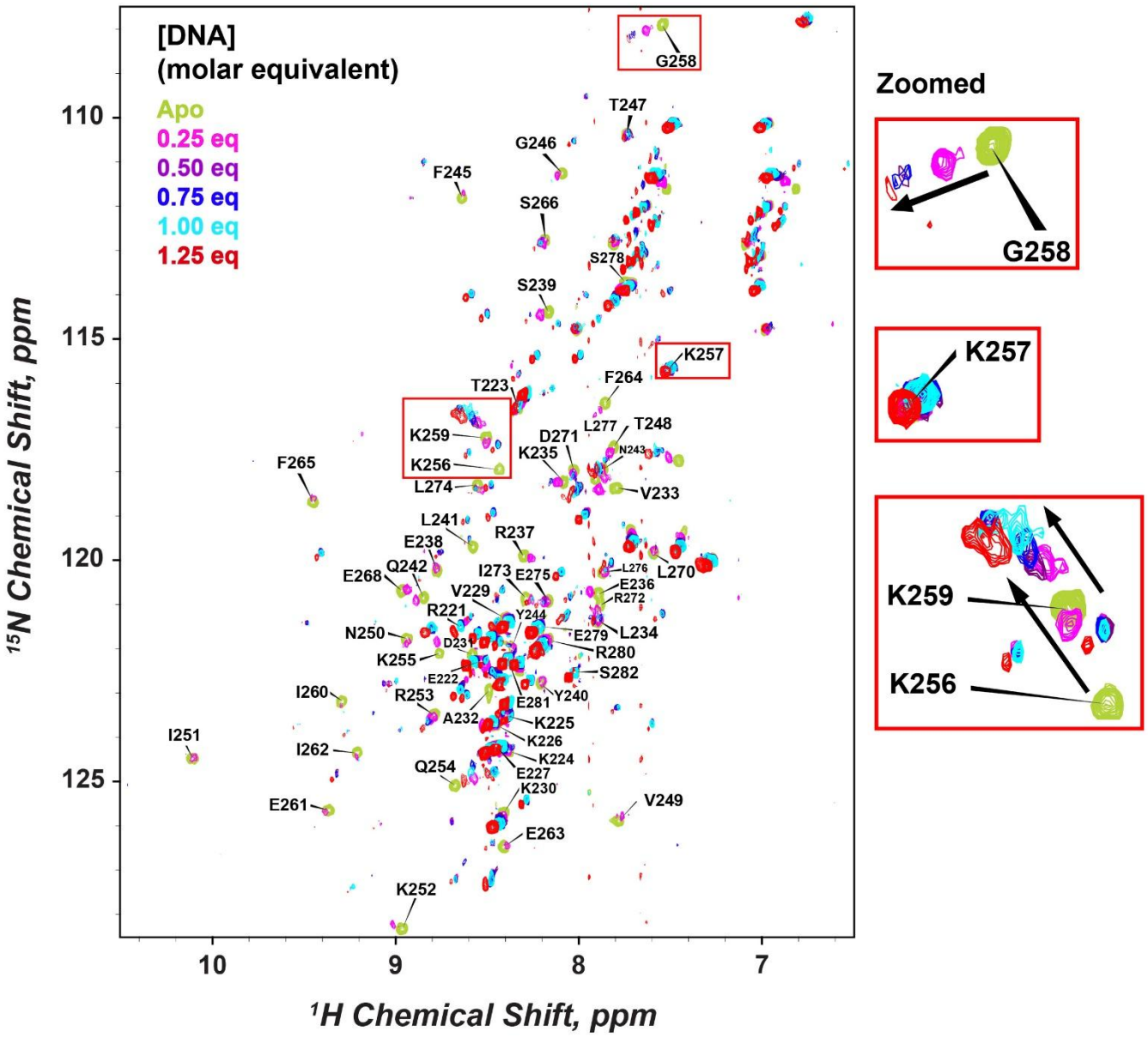

Figure S6. ^{1}H-^{15}N HSQC spectra of 250 μM CTD at 11.7 T in PBS buffer, pH 6.1 at 308 K titrated with increasing concentrations of 10 bp hairpin DNA.

Several residues exhibiting high (K256, G258, and K259) and low (K257) chemical shift perturbations are shown at higher magnification in the red boxes. Several residues are shown at higher magnification within the red boxes to illustrate varying degrees of chemical shift perturbation. Arrows indicate the approximate directions of spectral transitions upon DNA binding.

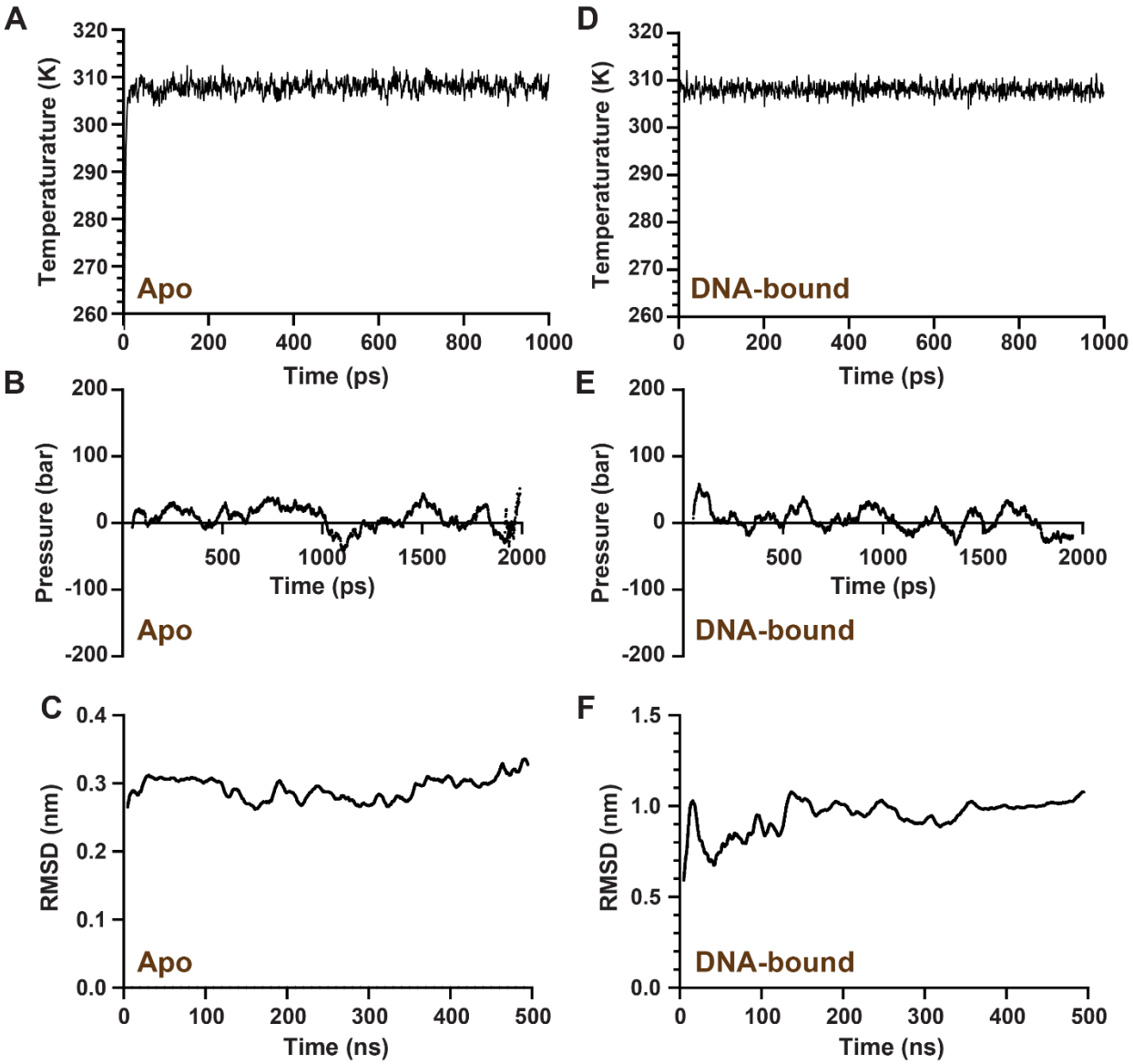

Figure S7. Analysis of the MD simulations during different phases

(**A** and **D**) Equilibration of temperature under the number of particles, volume, and temperature (NVT ensemble) conditions for (**A**) apo and (**D**) DNA-bound CTD.

(**B** and **E**) Equilibration of pressure under the number of particles, pressure, and temperature (NPT ensemble) conditions for (**B**) apo and (**E**) DNA-bound CTD.

(**C** and **F**) RMSD analysis of the MD production phase for (**C**) apo and (**F**) DNA-bound CTD.

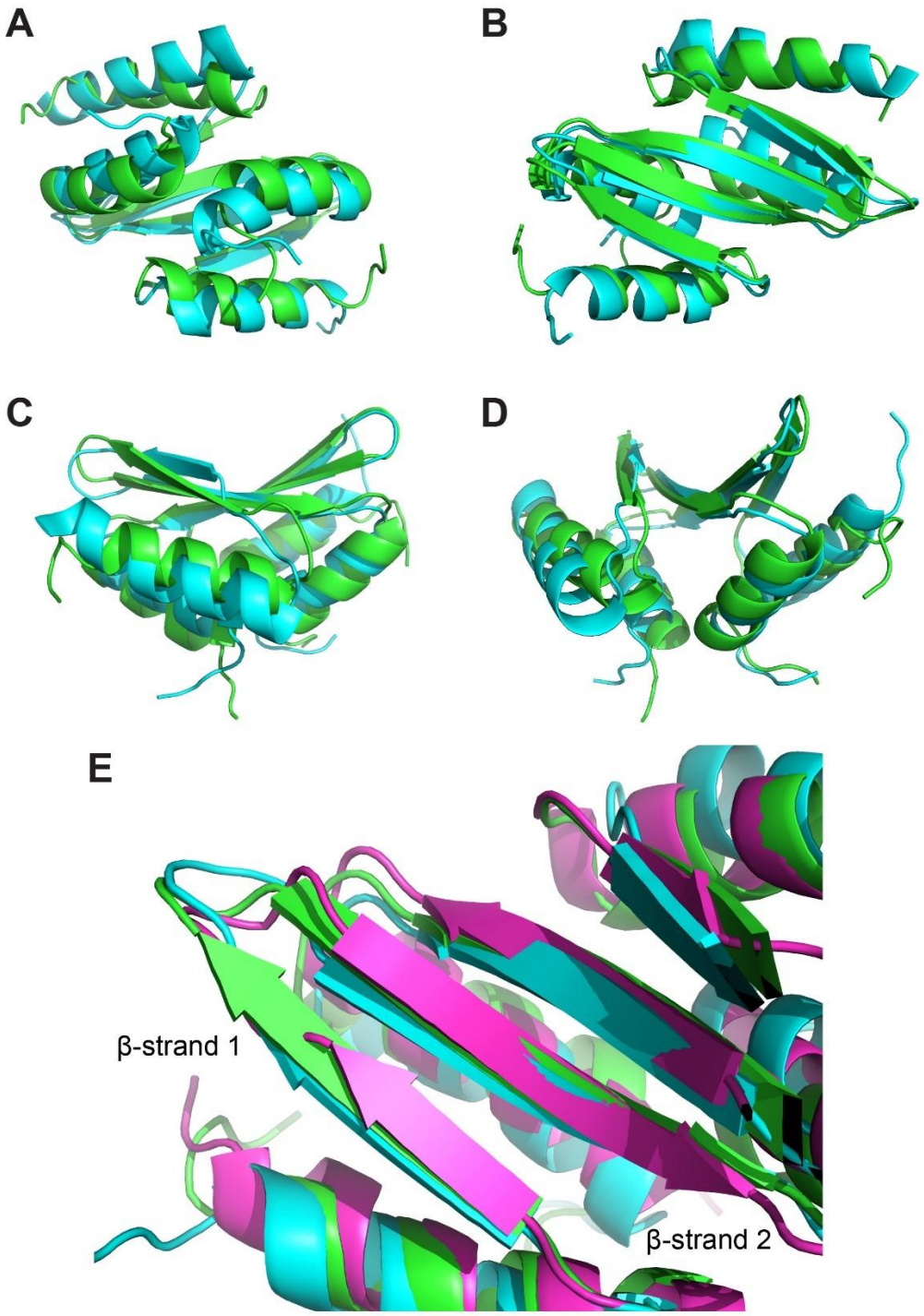

Figure S8. An overlay of the ParB C-terminal domain (CTD) structures

(**A**-**D**) An overlay of average simulated apo CTD (green) and DNA-bound CTD (cyan) structures. Views from (**A**) the bottom, (**B**) the top, (**C**) the side, and (**D**) the front.

(**E**) Average simulated structures of apo (green) and DNA-bound CTD (cyan), along with apo NMR structure (PDF entry: 5NOC) (purple), are overlaid to highlight differences in β-strands. The NMR structure of DNA-bound CTD is not available.

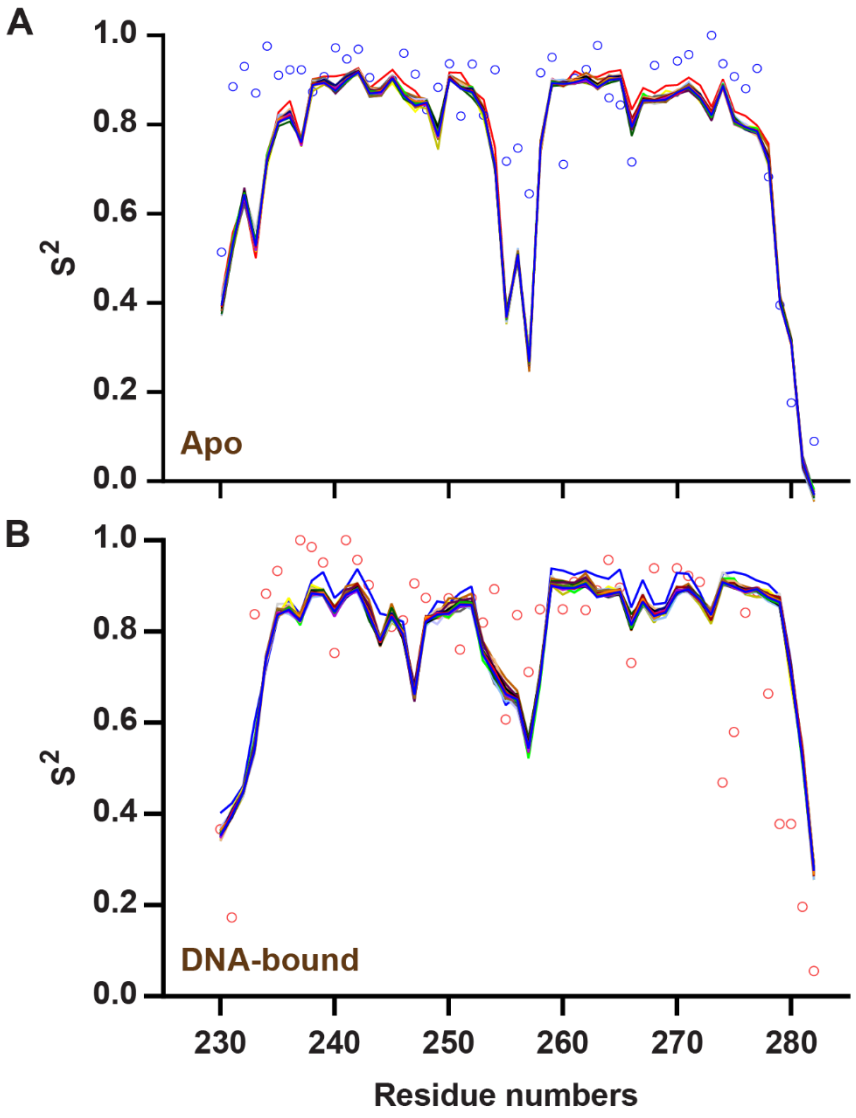

Figure S9. Generalized order parameter (S^2) comparison

(**A**) Experimental (model-free values) versus computer-simulated (from 500 ns MD trajectories with averaging time windows from 100 ps to 5 ns) S^2 values for apo CTD. The open circles represent experimental model-free S^2 values, and the solid lines represent molecular dynamics simulation results. (**B**) Those for DNA-bound SCTD.

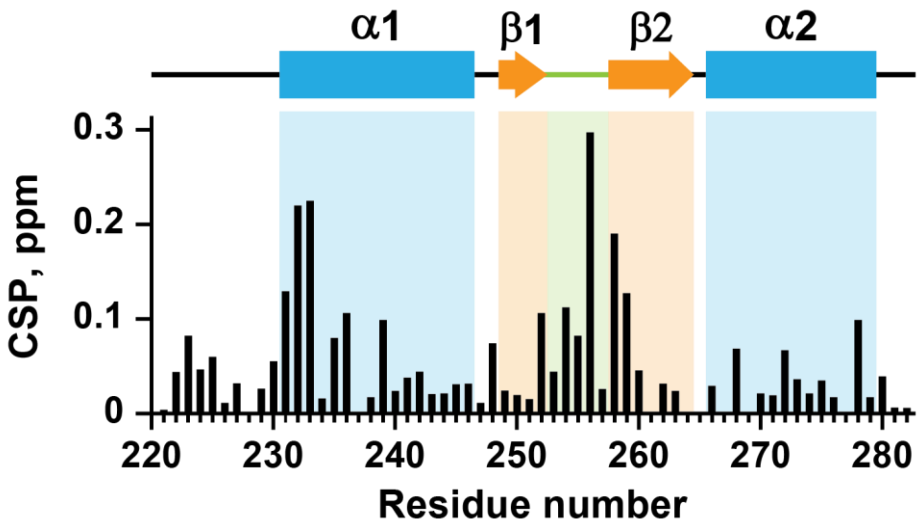

Figure S10. Chemical shift perturbation (CSP) of CTD upon addition DNA, at pH 6.1, 0.4 mM

The secondary structure of the apo CTD determined from the NMR structure (PDB: 5NOC) is displayed at the top: α-helices (blue bars), β-strands (orange arrows), loop regions (black lines), and linker region (green).

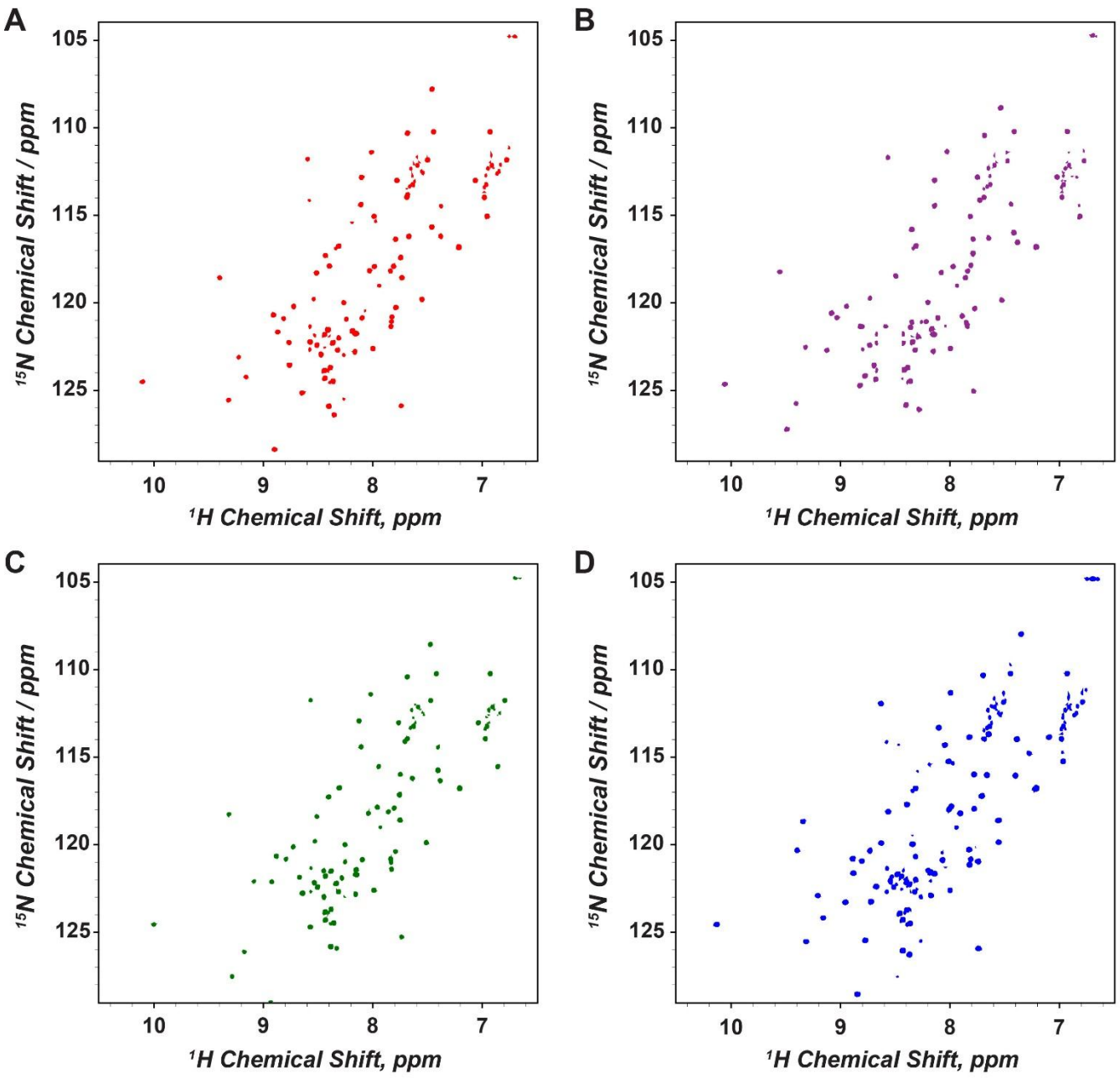

Figure S11. ^{1}H-^{15}N HSQC spectra of apo-CTD.

The spectra for (**A**) wild-type, (**B**) K256A, (**C**) K259A, and (**D**) KKK (K252A-K255A-K259A) C-terminal domain were obtained at 11.7 T with 135 μM CTD in PBS buffer, pH 6.1, at 308 K.

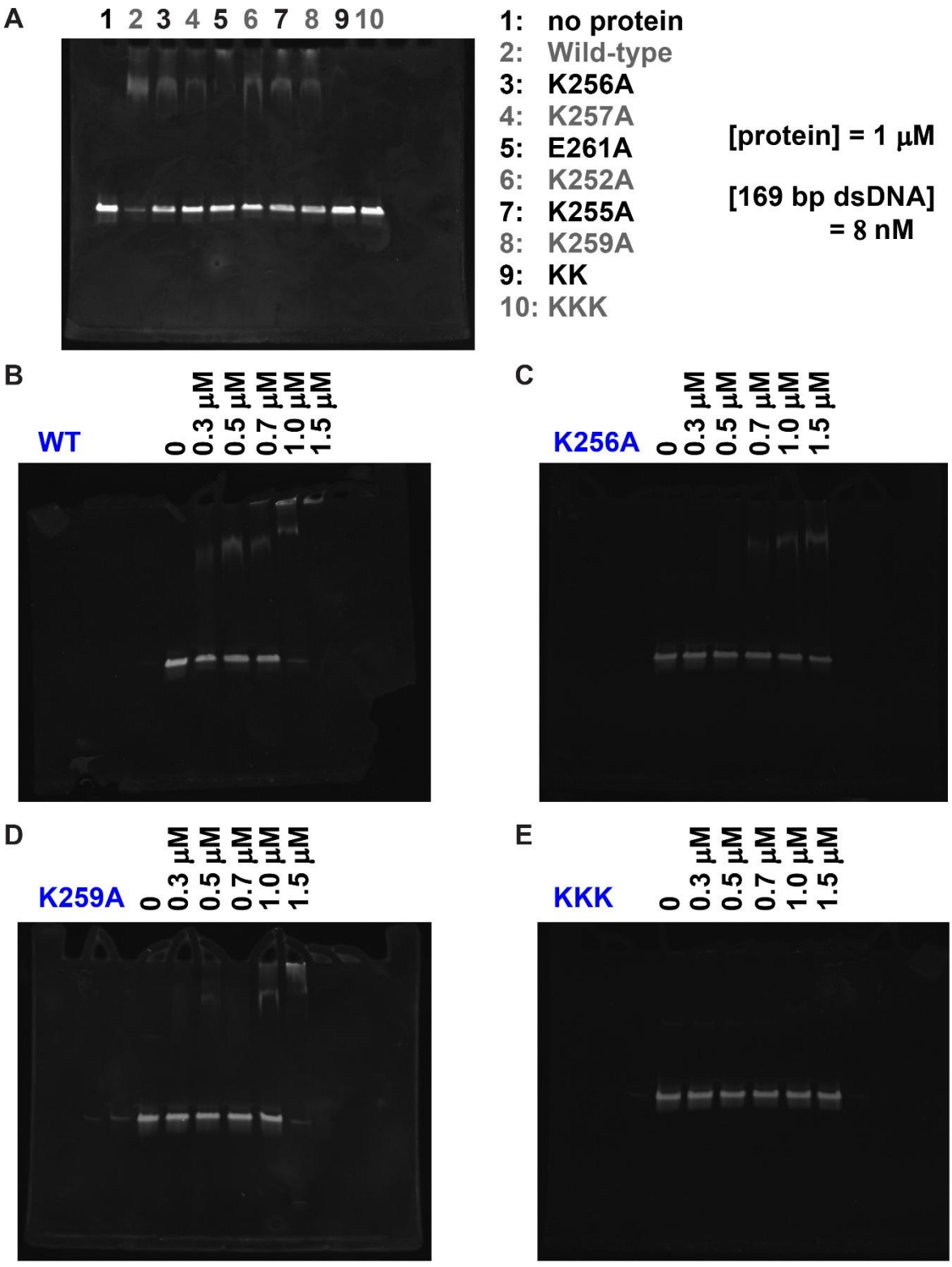

Figure S12. Representative (unprocessed) raw images of electrophoretic mobility shift assay (EMSA) (*N*=3). KK and KKK represent K252A-K259A and K252A-K255A-K259A mutant proteins, respectively. (**A**) EMSA with wild-type and (full-length) C-terminal domain mutant *B. subtilis* ParB (BsParB) proteins. (**B-E**) EMSA with increasing concentrations of (**B**) wild-type, (**C**) K256A, (**D**) K259A, and (**E**) KKK BsParB proteins.

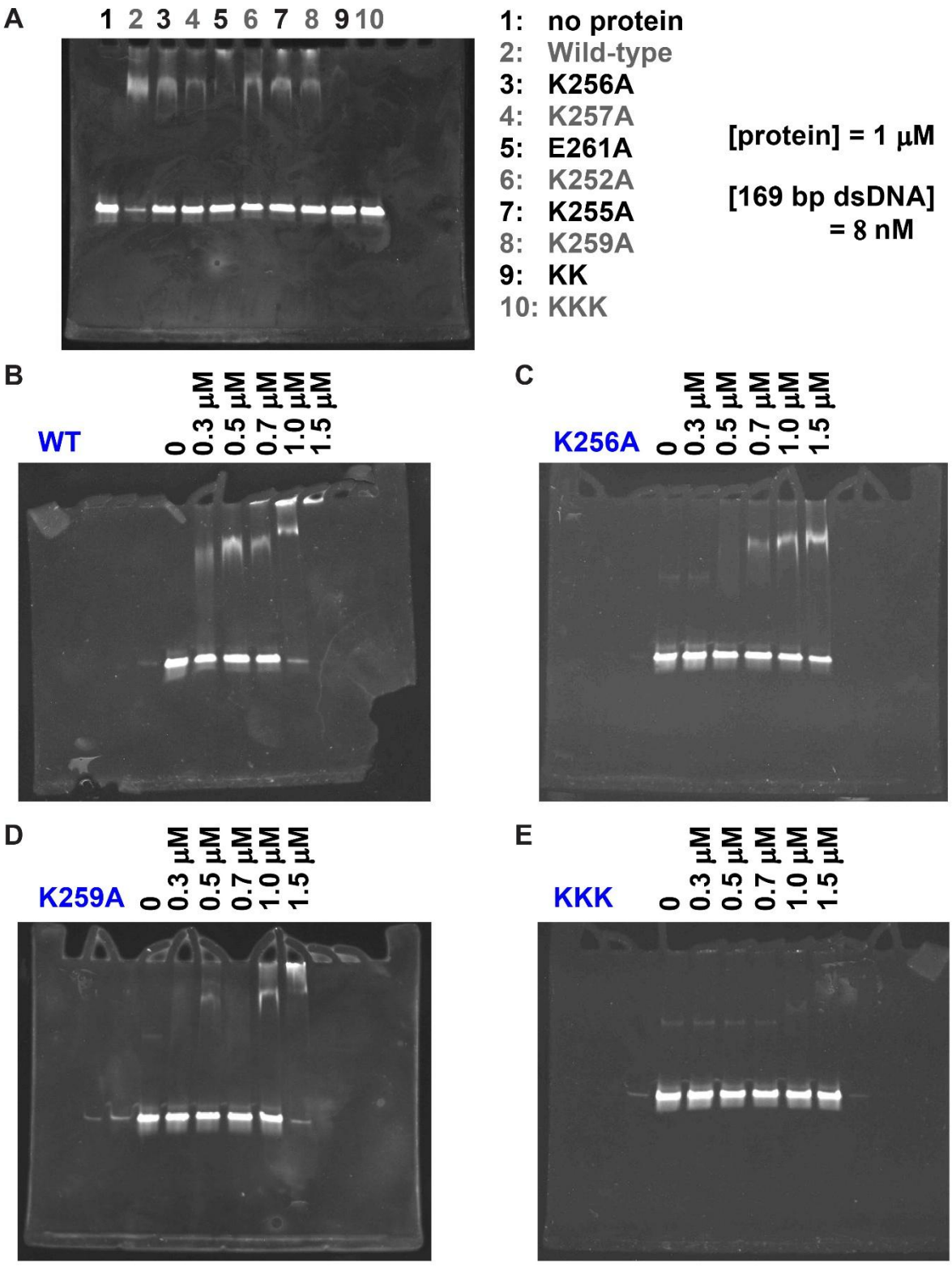

Figure S13. Brightness-adjusted images of electrophoretic mobility shift assay (EMSA) (*N*=3). KK and KKK represent K252A-K259A and K252A-K255A-K259A mutant proteins, respectively.
(**A-E**) Same as **Figure S12**.

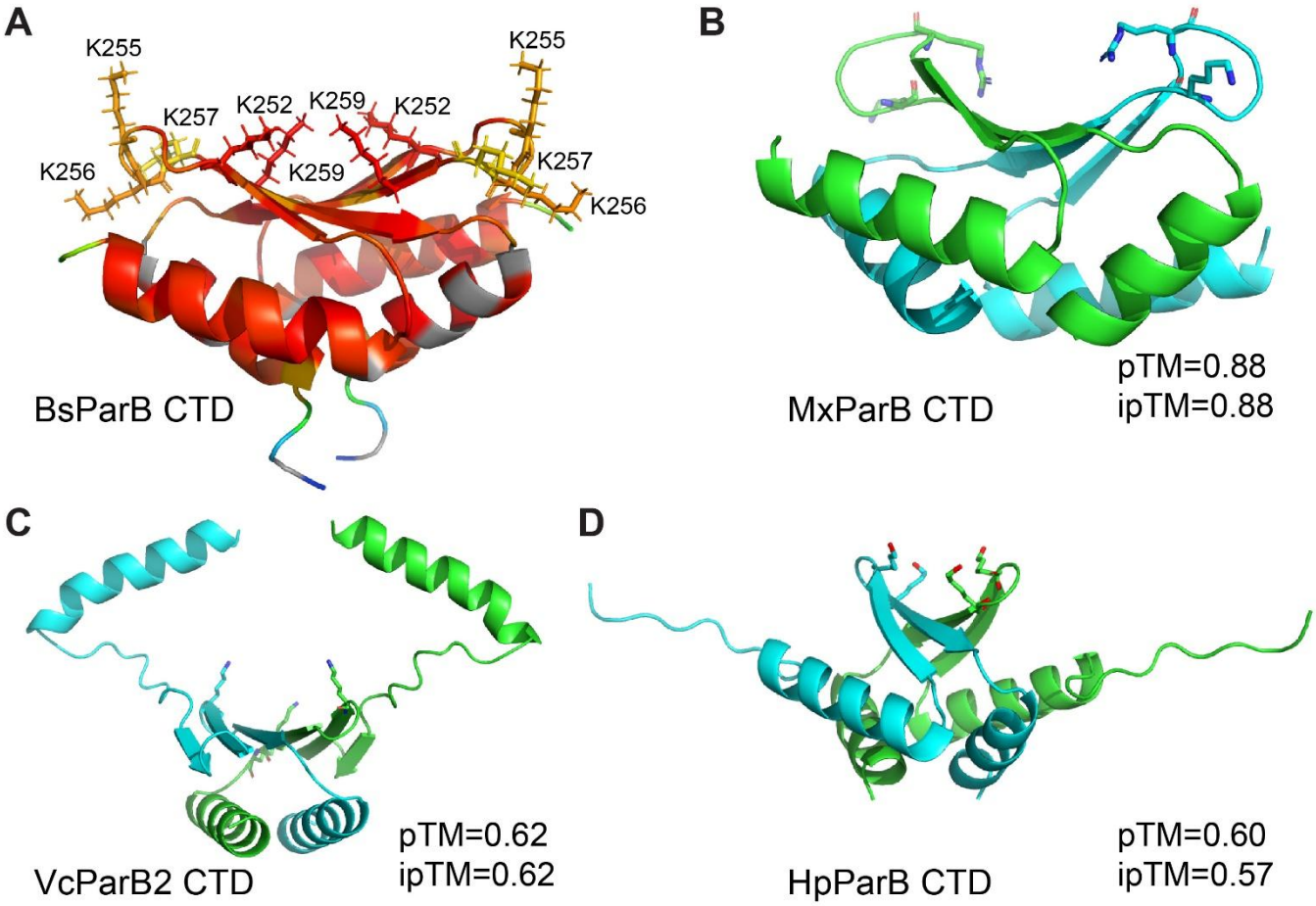

Figure S14. AlphaFold 3 predictions of chromosomal ParB C-terminal domain (CTD).
(**A**) An NMR structure of the *Bacillus subtilis* ParB (BsParB) CTD (PDB entry: 5NOC) to compare with those in other organisms. This figure is adopted from **Figures 2C** and **S5A**.
(**B-D**) AlphaFold3 [1] predictions of (**B**) *Myxococcus xanthus* ParB (MxParB), (**C**) *Vibrio cholerae* ParB (VcParB2), and (**D**) *Helicobacter pylori* ParB (HpParB) CTD. Cyan and green represent the two monomers. pTM and ipTM denote the predicted template modeling and the interface predicted template modeling scores, respectively. Some positively charged residues are shown in stick representation to highlight their orientations.

References for the SI Figures

1. Abramson,J., Adler,J., Dunger,J., Evans,R., *et al.* (2024) Accurate structure prediction of biomolecular interactions with AlphaFold 3. *Nature*, 630, 493–500.

2. Madeira,F., Madhusoodanan,N., Lee,J., Eusebi,A., *et al.* (2024) The EMBL-EBI Job Dispatcher sequence analysis tools framework in 2024. *Nucleic Acids Res*, 52, W521–W525.

3. Waterhouse,A.M., Procter,J.B., Martin,D.M.A., Clamp,M., *et al.* (2009) Jalview Version 2--a multiple sequence alignment editor and analysis workbench. *Bioinformatics*, 25, 1189–1191.